AIAA 2001-2622

Parallel Residual Distribution Solver for the Ideal 3D Magnetohydrodynamic Equations: Applications to Flows in Space Physics

Árpád Csík[1,2], Hans de Sterck[3], Bart van der Holst[2], Herman Deconinck[1], Stefaan Poedts[2]

[1] *von Karman Institute for Fluid Dynamics, Waterloosesteenweg 72, Sint-Genesius-Rode, B-1640, Belgium*

[2] *Katholic University of Leuven, Department of Mathematics, Celestijnenlaan 200B, Heverlee, B-3001, Belgium*

[3] *University of Colorado at Boulder, Department of Computer Science, Campus Box 430, Boulder, Colorado 80309-0430, USA*

15th AIAA Computational Fluid Dynamics Conference

11-14 June 2001 Anaheim, CA

Parallel Residual Distribution Solver for the Ideal 3D Magnetohydrodynamic Equations: Applications to Flows in Space Physics

Árpád Csík[1,2]*, Hans de Sterck[3]†, Bart van der Holst[2]‡,
Herman Deconinck[1]§, Stefaan Poedts[2]¶

[1] *von Karman Institute for Fluid Dynamics, Waterloosesteenweg 72, Sint-Genesius-Rode, B-1640, Belgium*
[2] *Katholic University of Leuven, Department of Mathematics, Celestijnenlaan 200B, Heverlee, B-3001, Belgium*
[3] *University of Colorado at Boulder, Department of Computer Science, Campus Box 430, Boulder, Colorado 80309-0430, USA*

Multidimensional upwind residual distribution schemes for the numerical solution of the ideal magnetohydrodynamics equations have been extended to three spatial dimensions. The schemes operate on unstructured grids composed of tetrahedra. Both the two and the three dimensional schemes have been implemented into a multipurpose parallel implicit solver. The code is used to investigate a complex interacting shock structure, involving intermediate shock segments appearing in a bow shock flow in space physics.

Introduction

The ideal magnetohydrodynamics (MHD) equations serve as a useful model for the description of many problems in the field of astrophysics. The set of ideal MHD equations forms a system of highly nonlinear conservation laws, therefore the solution of more complicated problems require the use of numerical methods.

In the paper of Csík, Deconinck and Poedts[1,2] (in what follows CSDP) the authors developed fluctuation splitting or residual distribution ($\mathcal{RD}$) schemes for the solution of the ideal MHD equations in two spatial dimensions. These schemes operate on an arbitrary unstructured triangulation of the computational domain, assuming piecewise linear variation of a certain set of variables. From computational point of view an attractive feature of the $\mathcal{RD}$ method is that a time step is constructed as a loop over all of the elements, and the numerical procedure in a given element does not require any information outside of this element. This results in a very compact stencil containing only the nearest neighbours of a node which makes an efficient parallel and implicit coding. From the theoretical side, $\mathcal{RD}$ schemes incorporate multidimensional upwind information derived from physical considerations. For more information on the $\mathcal{RD}$ schemes see the recent review paper of Deconinck *et al.*[3]

In the present paper we extend the 2D schemes of CSDP to three spatial dimensions and apply them to the simulation of MHD flows relevant to space physics. Both the 2D and the 3D schemes have been implemented into the multipurpose VKI flow solver called THOR, which will be used to perform the numerical experiments.

The structure of the paper is as follows. After the introduction, in section two we describe the governing equations of ideal MHD. In the third section we recall the basic principles of the $\mathcal{RD}$ method and we outline the solution procedure. In the fourth section we give a brief description of the THOR code. In the fifth section we present a test problem and the solution of a steady magnetized bow shock flow involving a complex structure of interacting shock segments. In the last section we give some concluding remarks.

The governing equations of ideal MHD

The hyperbolic system of the single fluid ideal MHD equations in conservative form is given by:

*Ph.D. Candidate, Department of Aeronautics and Aerospace, Center for Plasma Astrophysics; arpi@vki.ac.be
†Post-doctoral researcher; desterck@babbage.colorado.edu
‡Post-doctoral researcher, Center for Plasma Astrophysics; Bart.vanderHolst@wis.kuleuven.ac.be
§Professor, AIAA member, Head of the Department of Aeronautics and Aerospace; deconinck@vki.ac.be
¶Professor, Research Associate of the F.W.O.-vlaanderen, Center for Plasma Astrophysics; Stefaan.Poedts@wis.kuleuven.ac.be

$$\frac{\partial U}{\partial t} + \nabla \cdot \mathbf{F} = 0 \tag{1}$$

where the conservative state vector U and the flux vector $\mathbf{F}$ containing the isotropic pressure tensor are:

$$U = [\rho, \rho u, \rho v, \rho w, B_x, B_y, B_z, E]^T \tag{2}$$

and

$$\mathbf{F} = \begin{pmatrix} \rho \mathbf{u} \\ \rho \mathbf{u}\mathbf{u} + \hat{I}(p + \mathbf{B} \cdot \mathbf{B}/2) - \mathbf{B}\mathbf{B} \\ \mathbf{u}\mathbf{B} - \mathbf{B}\mathbf{u} \\ (E + p + \mathbf{B} \cdot \mathbf{B}/2)\mathbf{u} - \mathbf{B}(\mathbf{u} \cdot \mathbf{B}) \end{pmatrix} \tag{3}$$

Here, $\hat{I}$ represents the 3×3 identity matrix, ρ is the density, u, v, and w are the x, y, and z components of the velocity vector $\mathbf{u}$, respectively, $\mathbf{B}$ is the magnetic induction vector, p is the thermal pressure, and E is the total energy density defined by

$$E = \frac{p}{\gamma - 1} + \frac{1}{2}\rho \mathbf{v} \cdot \mathbf{v} + \frac{1}{2}\mathbf{B} \cdot \mathbf{B}$$

where γ is the ratio of specific heats. Equation (1) describes the conservativion of mass, momentum, magnetic flux and energy and is to be supplemented by the divergence free condition of the magnetic field:

$$\nabla \cdot \mathbf{B} = 0 \tag{4}$$

Equation (4) is an initial constraint which is preserved in an analytic treatment if it is initially satisfied. However, in the course of the numerical solution of the MHD equations $\nabla \cdot \mathbf{B}$ may deviate from zero, which has a destabilizing effect on a numerical algorithm. Therefore a special care has to be taken to avoid the appearance of magnetic monopoles, or to stabilize the scheme against nonzero $\nabla \cdot \mathbf{B}$. There are three most often used methods to overcome this problem.

The original work of Evans and Hawley[4] is based on the observation that the induction equation should be discretized in a form which describes the temporal variation of the magnetic flux across a surface element, rather than the magnetic field itself. There are several implementations of this basic concept to maintain the solenoidal condition of the magnetic field up to machine accuracy in a certain discretization.[5] However, all of these schemes operate on structured Cartesian or curvilinear grids and they do not extend to irregular structured and other unstructured meshes.

The projection method is an often used tool to remove the solenoidal component of the magnetic field generated by the numerical scheme. Although in certain cases the projection method is proven to be working,[5] its highly inconsistent nature with the hyperbolic MHD equations prevents it from being useful in several other applications. Thus, the projection method is not considered further in this paper.

In order to stabilize the $\mathcal{RD}$ schemes against the instability due to the numerically generated nonzero divergence of the magnetic field, we employ the solution technique first proposed by Powell *et al.*,[6] in which a nonconservative source term is added to the right hand side of conservation law (1). In 1972 it was shown by Godunov,[7] that the resulting set of equations is the unique symmetrizable form of the ideal MHD equations:

$$\frac{\partial U}{\partial t} + \nabla \cdot \mathbf{F} = S \tag{5}$$

where $S = -[0, B_x, B_y, B_z, u, v, w, \mathbf{u} \cdot \mathbf{B}]^T \nabla \cdot \mathbf{B}$. Although equations (1) and (5) are identical at the analytic level, experience has shown, that the numerical solution of equation (5) is much more stable and robust. In this formulation the solenoidal condition is not strongly enforced, therefore $\nabla \cdot \mathbf{B}$ may deviate from zero. Consequently, the presence of the nonconservative source term S may lead to inconsistent jumps accross discontinuities. Indeed, Toth presented computational evidence[5] showing that the numerical solution of equation (5) converges to wrong jumps across the fast shocks present in that specific problem. However, the eight wave formulation has been tested on a wide range of problems and succesfully used in many astrophysical applications.[1,8–10]

In the quasilinear form of equation (5) the source term S can be incorporated into the singular Jacobian matrices $\partial F_x/\partial U$, $\partial F_y/\partial U$ and $\partial F_z/\partial U$, giving

$$\frac{\partial U}{\partial t} + A_U \frac{\partial U}{\partial x} + B_U \frac{\partial U}{\partial y} + C_U \frac{\partial U}{\partial z} = 0 \tag{6}$$

where A_U, B_U and C_U are the regularized Jacobian matrices (see CSDP).

Fluctuation Splitting Spatial Discretisation

In this section we briefly describe the $\mathcal{RD}$ method particularly for the ideal MHD equations in three spatial dimensions, which is a direct extension of the 2D schemes developed in CSDP.

We solve the eight-wave equations (5) of ideal MHD over spatial domain Ω devided into non overlapping tetrahedra. The geometry of an elementary tetrahedron using local nodal indices $j \in [1, 2, 3, 4]$ is shown in figure 1. The inward pointing normal vector $\mathbf{n_j}$ is scaled with the area of the face opposite to node j.

The solution over Ω is approximated by a continuous piecewise linear function, just like in linear finite element menthods:

$$U(x,y,z,t) = \sum_{i=1}^{N} U_i(t) w_i(x,y,z)$$

where N is the total number of nodes in the mesh, $U_i(t)$ is the time dependent value $U(x_i, y_i, z_i, t)$ at node i, and the piecewise linear shape function $w_i(x,y,z)$ equals to unity at node i and vanishes outside the support of all tetrahedra meeting at node i. Consequently, the components of the state vector U vary linearly in each element.

Integration of equation (6) yields the definition of the cell residual or total fluctuation Φ^T in tetrahedron T:

$$\begin{aligned}\Phi^T &= -\int_T \frac{\partial U}{\partial t}\, d\Omega = \int_T (\nabla \cdot \mathbf{F} - S)\, d\Omega \\ &= \int_T \left(A_U \frac{\partial U}{\partial x} + B_U \frac{\partial U}{\partial y} + C_U \frac{\partial U}{\partial z} \right) d\Omega \\ &= \left(\widehat{A_U}\mathbf{i} + \widehat{B_U}\mathbf{j} + \widehat{C_U}\mathbf{k} \right) \cdot \int_T \nabla U \, d\Omega\end{aligned}$$

where $\widehat{A}_U$, $\widehat{B}_U$ and $\widehat{C}_U$ are constant matrices in each tetrahedron taken in an appropriate averaged state $\bar{U}$. Since the variation of the conservative state vector U is linear in tetrahedron T, Φ^T can be expressed as

$$\Phi^T = \sum_{j=1}^{4} K_j U_j \tag{7}$$

Here index j goes through the local node numbers of element T, U_j is the solution at node j, and K_j is defined by the following linear combination of the Jacobians:

$$K_j = \frac{1}{3}(\widehat{A}_U\mathbf{i} + \widehat{B}_U\mathbf{j} + \widehat{C}_U\mathbf{k}) \cdot \mathbf{n_j}$$

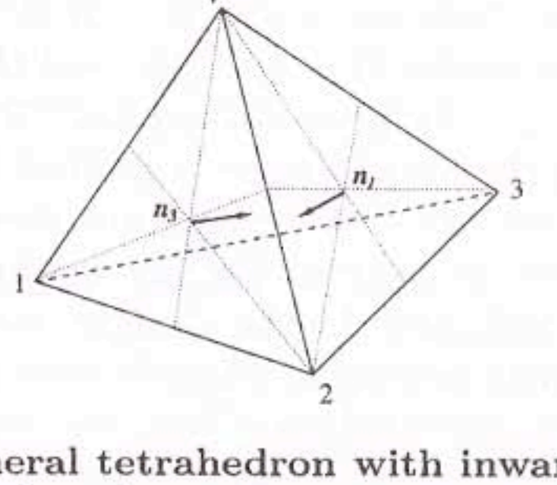

Fig. 1 General tetrahedron with inward pointing scaled normal vectors $\mathbf{n_j}$.

Matrix K_j has real eigenvalues and a complete set of left and right real eigenvectors, which can be appropriately scaled in order to remove the degeneraties present in the original form.[6,11–13] Diagonalization of matrix K_j yields:

$$K_j = \frac{1}{3} R_j \Lambda_j L_j \tag{8}$$

where the columns of R_j contain the scaled right eigenvectors, the rows of L_j contain the scaled left eigenvectors and Λ_j is the diagonal matrix of the eigenvalues proportional to $|\mathbf{n_j}|$. Matrices K_j^+ and K_j^- are the so called generalized upwind parameters, defined as

$$K_j^+ = \frac{1}{3} R_j \Lambda_j^+ L_j \text{ and } K_j^- = \frac{1}{3} R_j \Lambda_j^- L_j \tag{9}$$

Here Λ_j^+ and Λ_j^- contains the positive and the negative eigenvalues, respectively: $\Lambda_j^{\pm} = (\Lambda_j \pm |\Lambda_j|)/2$.

In the solution procedure of equation (6) first the cell residual Φ^T is computed in all the tetrahedra T and distributed to the nodes of T. The distribution function Φ_j^T is the fraction of the total cell residual distributed to node j in element T. For consistency we require that

$$\Phi_1^T + \Phi_2^T + \Phi_3^T + \Phi_4^T = \Phi^T \tag{10}$$

The fully multidimensional upwind property of the $\mathcal{RD}$ schemes implies that residual is not distributed to node j if all the eigenvalues of the corresponding matrix K_j is negative:

$$\Phi_j^T = 0 \text{ if } \Lambda_j^+ = \hat{0} \tag{11}$$

where $\hat{0}$ is the null matrix. The contributions Φ_j^T are assembled to compute the nodal update. This treatment leads to a very compact stencil, containing only the nearest neighbours of node j even for the second order accurate schemes. This property makes an efficient parallel implicit coding. The semi-discretised form of equation (6) at point j with the lumped Galerkin mass matrix is

$$\frac{dU_i}{dt} = -\frac{1}{V_i} \sum_{T, i \in T} \Phi_i^T \tag{12}$$

Here, V_i is the volume of the median dual cell around node i equal to one fourth of the volume of tetrahedra sharing node i.

The properties of the different schemes in the fluctuation splitting context are determined by the way Φ_i^T is defined. In this paper we use the first order linear monotone N scheme and the nonlinear B scheme which

is second order and monotone at the steady state. The corresponding distribution functions Φ_i^N and Φ_i^B are not given here, because they are trivial extensions of the 2D variant of these schemes (see CSDP).

The THOR code

In the last five years a software package has been developed at the Von Karman Institute for the numerical solution of conservation laws with source terms, based on the $\mathcal{RD}$ method. The THOR code is a 2D/3D parallel implicit solver written in C language. Due to its modular structure different equations can be easily integrated beside the Euler, turbulent Navier-Stokes and the ideal MHD equations. A powerful feature of the THOR code is that it operates on unstructured hybrid grids, thus allowing to use appropriate elements for specific flow structures (*e.g.* quadrilaterals with high aspect ratio can be used in viscous layers and triangles or tetrahedra in other domains). THOR contains automatic grid adaptation as an option, to follow and resolve fine structures in the flow filed in an economic manner. The THOR code expanded with the MHD modules was used in the computations presented in the next section.

Simulation Results and Discussion

Numerical experiments were performed on the IBM SP2 computer of the Katholic University of Leuven (KUL) using only 6 nodes connected by ethernet, each of them containing 4 processors.

Quasi-2D Nozzle flow

In order to test the implementation of the 3D $\mathcal{RD}$ MHD schemes and the performance of the parallel solution technique, we present the computation of a magnetized flow in a 3D nozzle. Super-magnetosonic flow enters the domain from the left, a shock developes in the converging part and the flow leaves at the right with a super-magnetosonic speed. At the back, front, top and bottom surfaces of the nozzle perfectly conducting ideal wall boundary conditions are imposed. The 3D grid is obtained by extruding the corresponding mesh of a 2D nozzle (see figure 2) into the direction normal to the 2D plane, then cutting the resulting prismatic elements into tetrahedra. The size of the 3D nozzle can be extended in the z direction by combining more layers of elements. A coarse 3D mesh containing 5 layers of tetrahedra is shown on figure 3 for visualization purpose only.

A simple test to check the 3D code is to solve a 2D problem on a 3D mesh and compare the result with the true 2D solution. In the initially imposed uniform flow field the density $\rho = 1$, the velocity vector $\mathbf{v} = (3, 0, 0)$, the magnetic induction vector $\mathbf{B} = (2, 0, 0)$, and the thermal pressure $p = 0.6$. Computations are done by the first order linear N scheme and the second order nonlinear B scheme with $CFL = 0.9$.

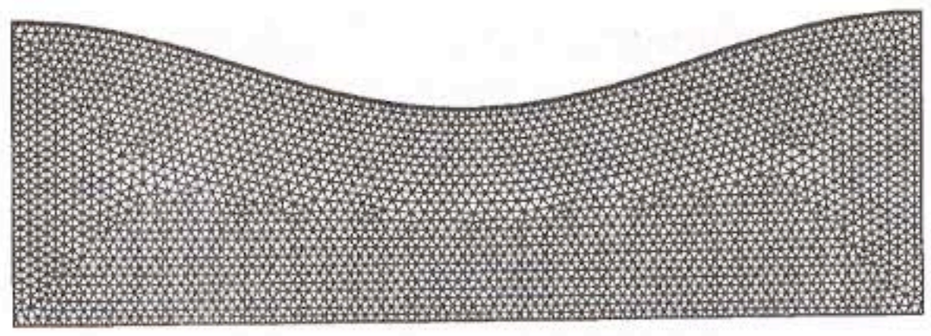

Fig. 2 Unstructured triangulation of a 2D nozzle containing 5.086 elements and 2.662 nodes. This grid serves as the basis of the 3D grid in the scaling problem and it was also used in the 2D computations.

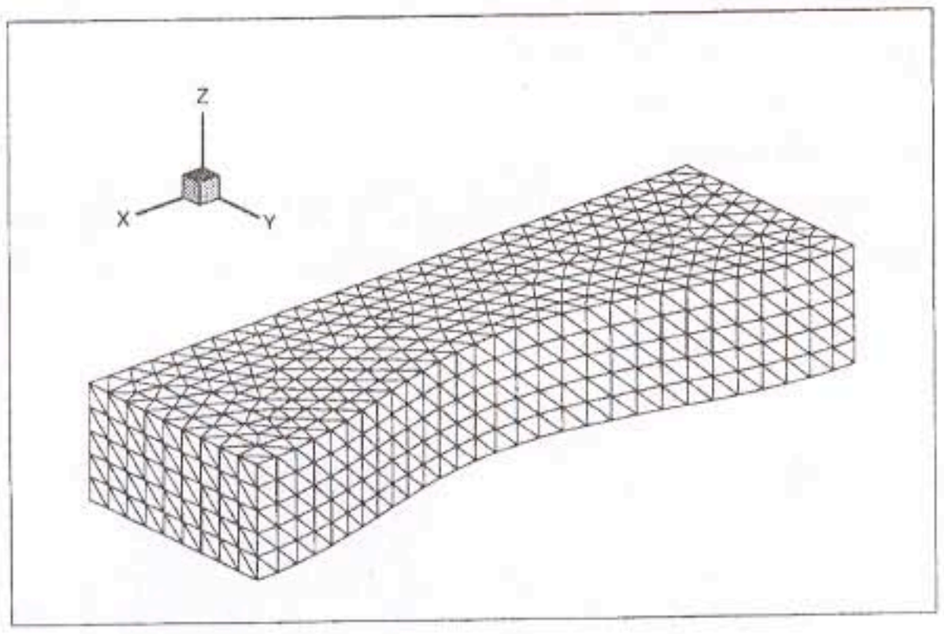

Fig. 3 A coarse grid for the 3D super-magnetosonic nozzle test case containing 5 layers of elements in the z direction.

The 3D steady state solution is plotted on figure 4 in a plane parallel to the $x - y$ plane. The density contour lines are superimposed by the magnetic field lines. The true 2D solution of the problem is shown on figure 5. The second order B scheme produces sharp shocks without spurious oscillations, while the first order N scheme gives more dissipative results. The 3D solution is slightly more diffusive than the 2D, due to the operation of the true multidimensional upwind $\mathcal{RD}$ schemes on the 3D mesh.

In order to perform the parallel scaling, we solve the 3D nozzle problem on 2, 4, 8, 16, and 24 processors such that the number of layers in the 3D grid equals to the number of processors (see table 1). This way the averaged workload of the processors is approximately the same for each computations. In the initially imposed uniform flow field we take a slightly different state than in the previous case: the density $\rho = 1$, the velocity vector $\mathbf{v} = (3, 0, 0)$, the magnetic induction vector $\mathbf{B} = (1, 0, 0)$, and the thermal pressure $p = 1$. On figure 6 the total CPU time required to reach the steady state is plotted versus the number of processors. In the ideal situation the total CPU time would be constant for any numbers of processors, which is indicated by the straight dashed line parallel to the horizontal axes. The relatively strong deviation of the experimental curve from the ideal line is mainly attributed to the following features of the hardware setup in the SP2 at KUL. First, the ethernet connec-

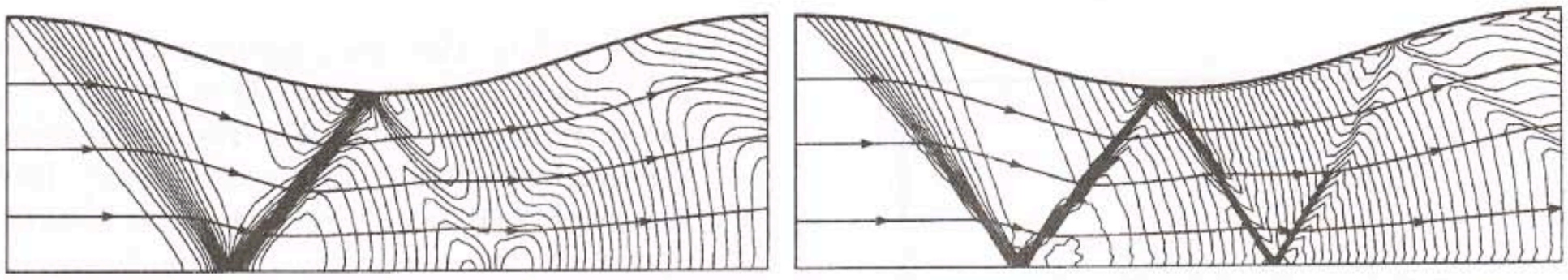

Fig. 4 Magnetic nozzle flow in 3D computed by the $\mathcal{RD}$ N (left) and B (right) schemes. Solution is shown in a plane parallel to the $x-y$ plane.

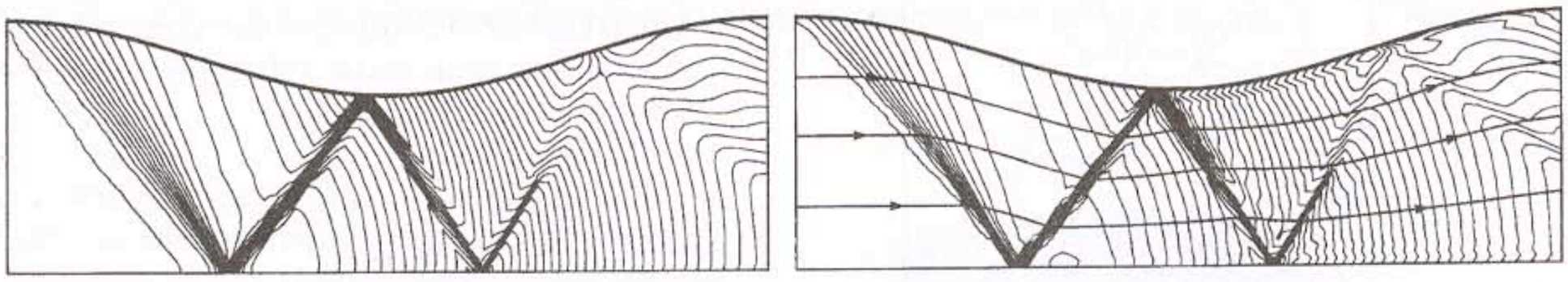

Fig. 5 Magnetic nozzle flow in 2D computed by the $\mathcal{RD}$ N (left) and B (right) schemes.

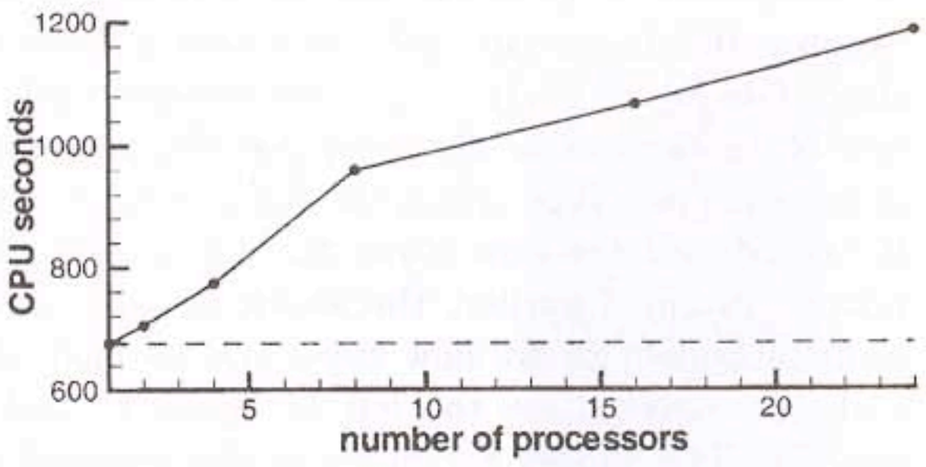

Fig. 6 Parallel scaling on the 3D magnetic nozzle test case. Total CPU time is plotted versus the number of processors. The straight dashed line indicates the *ideal* scaling.

tion between the nodes slows down the computation when more than four processors operate parallel. Second, the scaling plot is considerably affected by writing (the final solution) onto the hard disc, since this is a particularly slow process in this specific version of the SP2.

processors	elements	nodes
1	15.258	5.324
2	30.516	7.986
4	61.032	13.310
8	122.064	23.958
16	244.128	45.254
24	366.192	66.550

Table 1: Number of nodes and elements in the 3D grids used for the parallel scaling. The number of processors equals the number of layers of elements in the z direction.

Complex Bow Shock Flow Around a Sphere

MHD bow shocks can be found in Space Physics flows where the super-magnetosonic solar wind encounters planetary obstacles.[14–17] Recent simulations using a high-resolution Finite Volume ($\mathcal{FV}$) shock-capturing code[9] on structured grids have shown that 3D MHD bow shock flows exhibit a new complex double-front topology in a well-defined parameter regime in which the upstream magnetic field is strong enough.[15–17] This parameter regime is called the magnetically dominated regime, as opposed to the pressure-dominated regime in which a regular single-front bow shock flow occurs.

In the left of figure 10 we show a 3D simulation result of such a complex bow shock flow around a perfectly conducting sphere that was obtained by a $\mathcal{FV}$ code on a structured grid, containing 128.000 ($40 \times 80 \times 40$) volumes. The inflow is specified by three parameters, *i.e.* the plasma beta $\beta = 2\,p/B^2 = 0.4$, the Alfvénic Mach number in the x direction $M_{Ax} = v_x\sqrt{\rho}/B_x = 1.49$, and the angle between the velocity and magnetic fields $\theta_{vB} = 5°$. The radius of the sphere is taken as $r = 0.125$. In the upstream flow the magnetic field is aligned to the x-axis.

In the right of figure 10 we show the 3D simulation result of the same bow shock flow obtained by the new $\mathcal{RD}$ method on an unstructured grid consisting of 830.280 tetrahedral elements and 149.310 nodes. Figure 7 shows the structure of the mesh (coarser than the one used in the final simulation of figure 10) in the $x-y$ symmetry plane. The $\mathcal{RD}$ simulation result was obtained by using the system N scheme on 16 processors with explicit time integration and local timestepping. The reader can observe that the new $\mathcal{RD}$ code produces a result consistent with the earlier $\mathcal{FV}$ computations, confirming the new physical finding that MHD bow shock flows may consist of several consecutive interacting shock fronts.[15–17]

MHD shock types

The new bow shock topology involves shock front segments of all three MHD shock types. Corresponding to the three types of linear waves, the MHD equations allow for three different types of shocks, namely the fast, intermediate and slow shocks (see figure 8). All MHD shocks have the property of co-planarity, which means that the downstream magnetic field lies

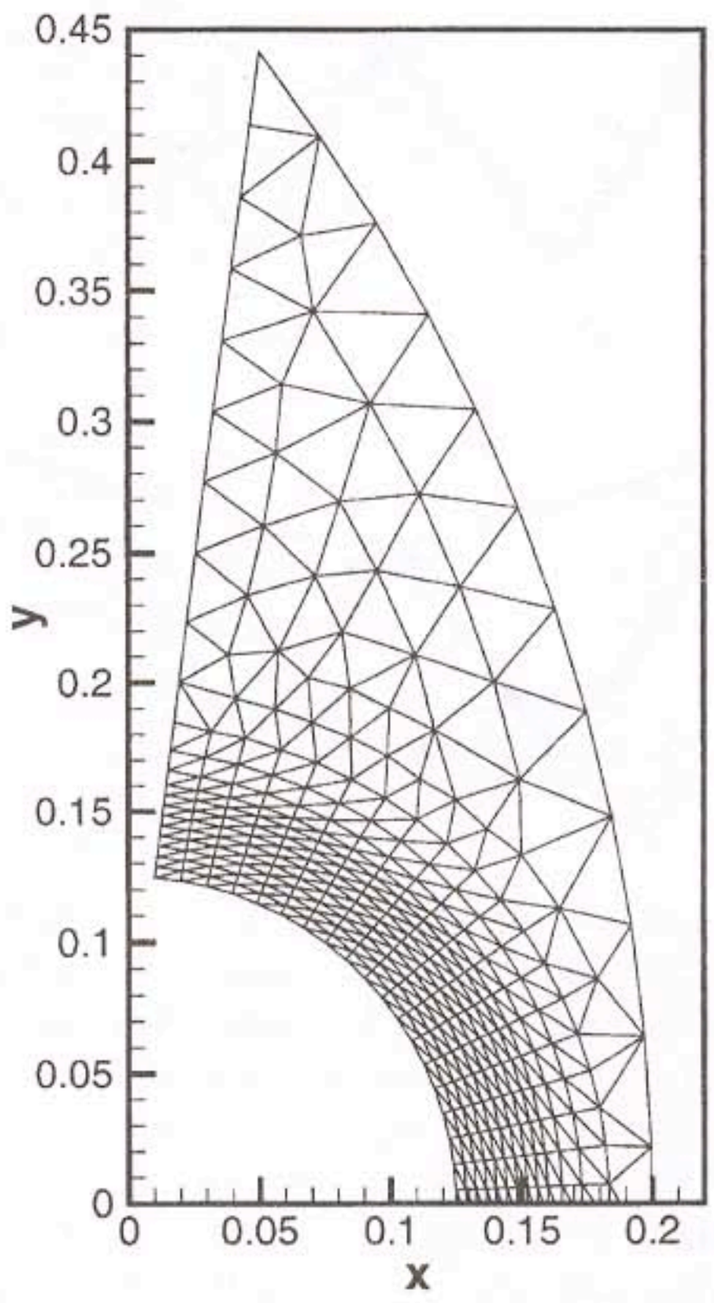

Fig. 7 2D unstructured triangular grid, obtained by a hybrid grid generator. This 2D mesh was used to construct the 3D tetrahedral grid for the bow shock simulations by an extrusion algorithm combined with rotation and stretching of the 2D grid.

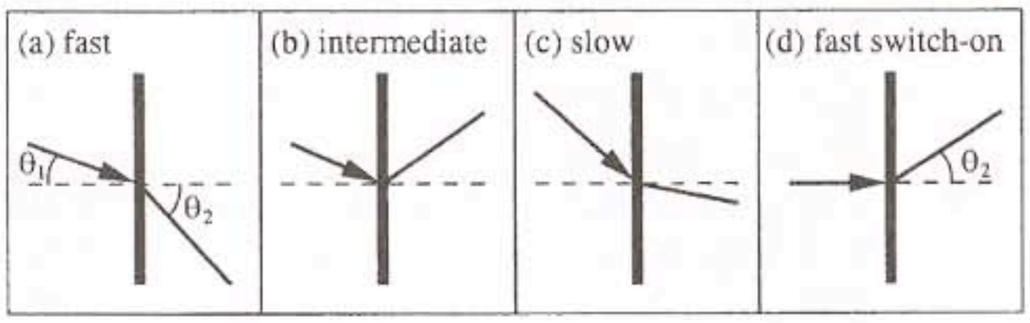

Fig. 8 The three types of MHD shocks (thick) refract the magnetic field (thin) in different ways. The shock normals are dashed. The left state is upstream, the right state is downstream. The switch-on shock (d) is a limiting case of the fast shock.

in the plane defined by the upstream magnetic field and the shock normal. Three types of shocks are thus described by the MHD equations, connecting plasma states which are traditionally labeled from 1 to 4, with state 1 a super-fast state ($v_n > c_{fn}$ in the shockframe, with n the direction of the shock normal), state 2 sub-fast but super-Alfvénic, state 3 sub-Alfvénic but super-slow, and state 4 sub-slow. The fast 1–2 shock transition brings a superfast upstream plasma to a subfast but super-Alfvénic downstream state, refracting the magnetic field away from the shock normal. A limiting case of the fast 1–2 shock is the 1–2=3 switch-on shock, for which the upstream magnetic field is parallel to the shock normal, while the magnetic field makes a finite angle with the shock normal in the downstream state. The tangential component of the magnetic field is thus switched on. Intermediate shocks (1–3, 1–4, 2–3 and 2–4) bring a super-Alfvénic upstream plasma to a sub-Alfvénic downstream state, while the magnetic field is flipped over the shock normal — the tangential component of the magnetic field changes sign. The slow 3–4 shock transition brings a superslow but sub-Alfvénic upstream plasma to a subslow downstream state, refracting the magnetic field towards the shock normal.

Shock topology

The simulation results of figure 10 are compared in more detail in figure 11, where cuts are shown in the $x - y$ symmetry plane. It can be seen that close to the primary shock segment the secondary shock is of intermediate MHD shock type in both computations, because the magnetic field lines switch back at the shock (see figure 8(b)). It is a remarkable result of the new $\mathcal{RD}$ schemes that the secondary shock seems to be of intermediate type *along its entire extent*, and that it extends *all the way along the sphere*. In the $\mathcal{FV}$ results obtained earlier, the shock seemed to switch from intermediate to slow type and seemed to have a shorter extent (see the left of figure 11 and reference[16]). The shocks are much better resolved in the $\mathcal{RD}$ simulations, and we can attribute this to the true multidimensional character of the schemes.[1,2] It is important to characterize the nature of the secondary shock in detail, and this remains an important topic for further investigation. In figure 12 we compare the flow in a plane perpendicular to the $x - y$ symmetry plane for the two simulation schemes.

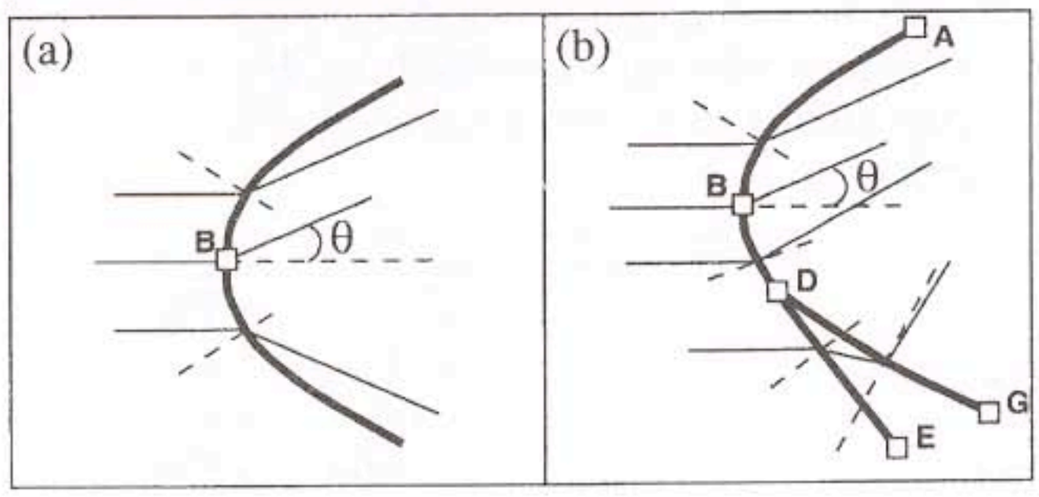

Fig. 9 (a) Sketch of a regular single-front bow shock topology. (b) The complex double-front topology that is obtained in our simulations with strong upstream magnetic field.

The shock fronts arising in figure 11 can be classified by using the labels on the diagram in figure 9(b). Regular bow shocks in the pressure-dominated regime have the classical single-front topology of figure 9(a), while the magnetically dominated bow shock flows discussed in the present paper have the topology of figure 9(b). The substantial difference between pressure-dominated and magnetically dominated MHD bow shock topologies can be explained in terms of the ge-

ometrical properties of MHD shocks.[17] Shock fronts AB and DE are 1–2 fast, and BD is 1–3 intermediate. The secondary shock segment DG is 2–4 intermediate, evolving into 3–4 slow along the front.[17]

Thus, part of the leading and secondary shock fronts are of intermediate MHD shock type. Intermediate MHD shocks are so-called overcompressive, non-Laxian shocks, in which more than one families of characteristics converge.[17] Intermediate shocks were believed to be inherently unstable until recently, but the simulations of figure 10 proved that they can exist and have to occur in real 3D MHD flows, confirming recent theoretical results on their stability when dissipation is finite (see Ref.[17] and references therein).

Conclusions

Multidimensional upwind $\mathcal{RD}$ schemes have been extended to the solution of the ideal MHD equations in three spatial dimensions on unstructured grids. The schemes have been implemented into the multi-purpose parallel implicit THOR solver.

The results demonstrate that our new $\mathcal{RD}$ N scheme is capable of capturing complex MHD shock interaction phenomena that involve different types of MHD shocks. At the same time, they confirm with an entirely different $\mathcal{FV}$ numerical technique,[9] that this new effect of secondary MHD shocks in bow shock flows is a true physical MHD effect. The results of the $\mathcal{RD}$ scheme indicate, that the secondary shock segment is of intermediate type along its entire length, unlike it was suggested by earlier computations.[15,17] The possible influence of the secondary shock and the associated switching back of the magnetic field lines on the reconnection process at the terrestrial magnetopause may be important for the physical processes that determine magnetic storms.[16]

The present $\mathcal{RD}$ results were obtained with the relatively dissipative system N scheme without the use of the solution adaptive algorithms of THOR. Simulation with the more accurate $\mathcal{RD}$ B scheme on finer adapted grids may lead to an increased understanding of the complex topology of these magnetically dominated bow shock flows.

Acknowledgement

These results were obtained in the framework of the project OT/98/14 (K.U.Leuven), G.0344.98 (FWO-Vlaanderen), and 14815/00/NL/SFe(IC) (ESA Prodex).

References

[1]Csík, Á., Deconinck, H., and Poedts, S., "Monotone Residual Distribution Schemes for the Ideal 2D Magnetohydrodynamic Equations on Unstructured Grids", *AIAA-CP 99-3325*, 1999, pp. 644-656.

[2]Csík, Á., Deconinck, H., and Poedts, S., "Monotone Residual Distribution Schemes for the Ideal Magnetohydrodynamic Equations on Unstructured Grids", *in press*, AIAA Journal, 2001.

[3]Deconinck, H., Sermeus, K., and Abgrall, R., "Status of Multidimensional Upwind Residual Distribution Schemes and Applications in Aeronautics", *AIAA-CP 2000-2328*, 2000.

[4]Evans, C.R., and Hawley, J.F., "Simulation of magnetohydrodynamic flows: a constrained transport method", *The Astrophysical Journal*, Vol. 332, 1988, pp. 659

[5]Toth, G., "The $\nabla \cdot B = 0$ Constraint in Shock-Capturing Magnetohydrodynamics Codes", *Journal of Computational Physics*, Vol. 161, 2000, pp. 605-652.

[6]Powell, K.G., Roe, P.L.,Myong, R.S., Gombosi, T., and Zeeuw, D., "An Upwind Scheme for Magnetohydrodynamics", *AIAA-CP 95-1704*, 1995.

[7]Godunov, S.K., "Nonlinear hyperbolic problems: Proceedings of an advanced research workshop", *Lecture Notes in Mathematics*, edited by Carasso, C., Raviart, P.A., Serre, D., Vol. 1270, Springer-Verlag, Berlin, 1987.

[8]Powell, K.G., Roe, P.L., Linde, T.J., Gombosi, T.I., and De Zeeuw, D.L., "A Solution-Adaptive Upwind Scheme for Ideal Magnetohydrodynamics", *Journal of Computational Physics*, Vol. 154, 1999, pp. 284-309.

[9]De Sterck, H., Csík, Á., Vanden Abeele, D., Poedts, S., and Deconinck, H., "Stationary two-dimensional magnetohydrodynamic flows with shocks: characteristic analysis and grid convergence study", *Journal of Computational Physics*, Vol. 166, No. 1, 2001, pp. 28.

[10]Harada, S., Hoffmann, K.A., Augustinus, J., "Numerical Solution of the Ideal Magnetohydrodynamic Equations for a Supersonic Channel Flow", *Journal of Thermophysics and Heat Transfer*, Vol. 12, No. 4, 1998, pp. 507-513.

[11]Brio, M., and Wu, C.C., "An Upwind Differencing Scheme for the Equations of Ideal Magnetohydrodynamics", *Journal of Computational Physics*, Vol. 75, 1988, pp. 400-422.

[12]Roe, P.L., and Balsara, D.L., "Notes on the Eigensystem of Magnetohydrodynamics", SIAM Journal, Applied Mathematics, Vol. 56, 1996, pp. 57-67.

[13]Barth, T.J., "An introduction to recent developments in theory and numerics for conservation laws", *Numerical methods for gasdynamics systems on unstructured meshes*, edited by Kröner, D., Ohlberger, M., and Rohde, C., Lecture notes in Computational Science and Engineering, Springer-Verlag, Berlin, 1998, pp. 195-284.

[14]Gombosi, T., I., *Physics of the Space Environment*, Cambridge University Press, Cambridge, 1999.

[15]De Sterck, H., *Numerical simulation and analysis of magnetically dominated MHD bow shock flows with applications in space physics*. PhD thesis, Katholieke Universiteit Leuven, Belgium, and National Center for Atmospheric Research, Boulder, Colorado, USA, 1999.

[16]De Sterck, H. and Poedts, S., "Stationary slow shocks in the magnetosheath for solar wind conditions with $\beta < 2/\gamma$: Three-dimensional MHD simulations", *J. Geophys. Res.*, 104(A10):22,401, 1999.

[17]De Sterck, H. and Poedts, S., Intermediate shocks in three-dimensional magnetohydrodynamic bow shock flows with multiple interacting shock fronts *Phys. Rev. Lett.*, 84(24):5524, 2000.

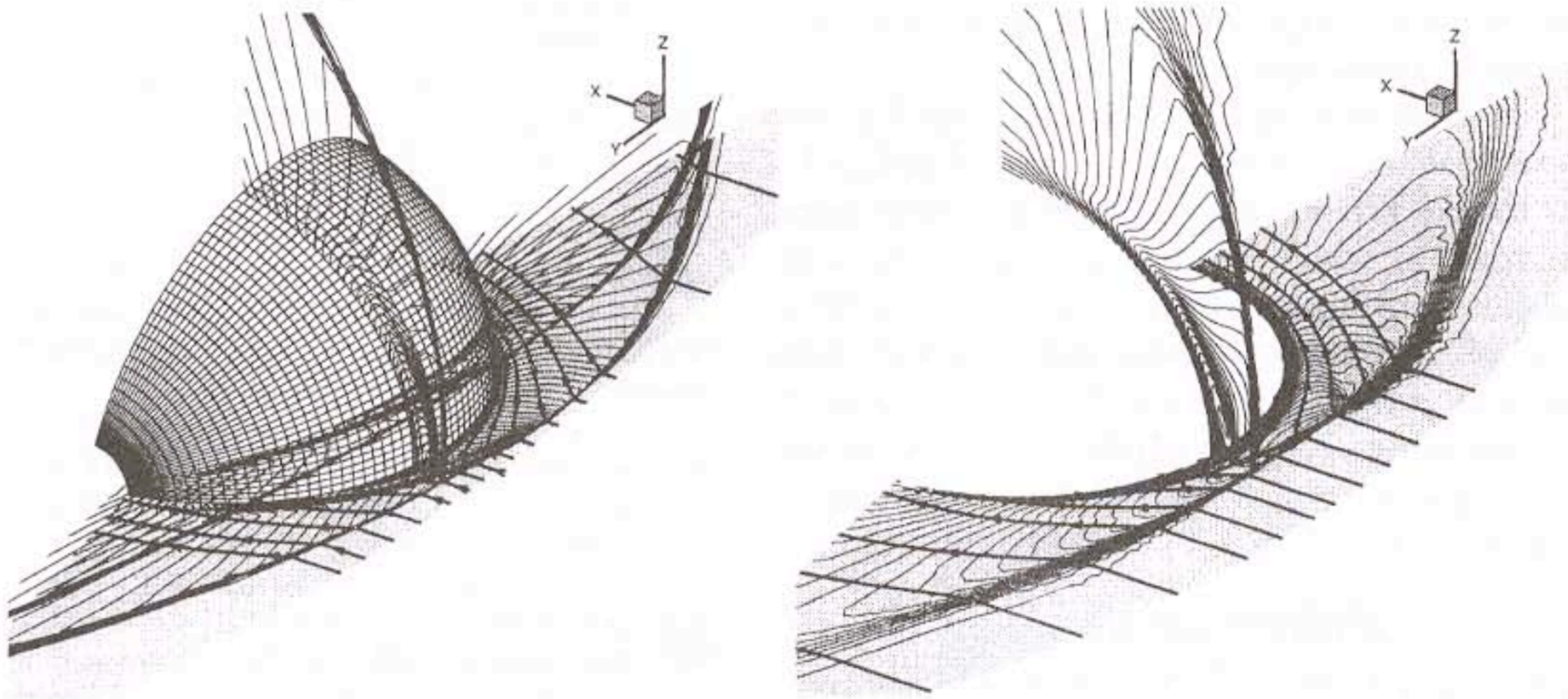

Fig. 10 Bow shock flow over a sphere computed by a second order MUSCL HLLEL $\mathcal{FV}$ scheme (left) and the first order $\mathcal{RD}$ N scheme (right). Density contours are superimposed by the magnetic field lines.

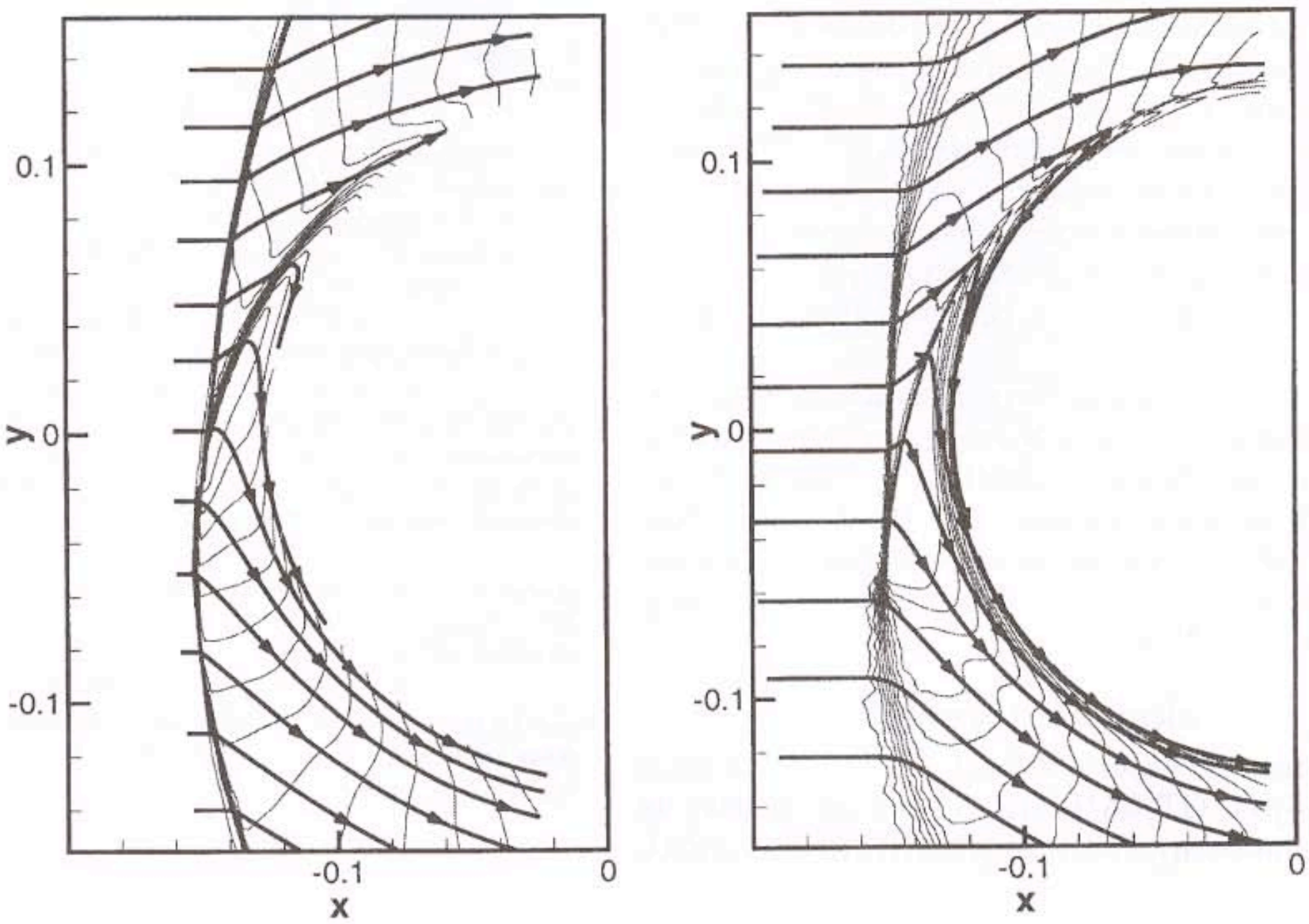

Fig. 11 Solution of the 3D bow shock flow in the $x-y$ symmetry plane computed by the $\mathcal{FV}$ (left) and the $\mathcal{RD}$ (right) schemes. Density contours are superimposed by the magnetic field lines. The new computation using the $\mathcal{RD}$ method indicates, that the secondary shock is of intermediate MHD shock type along its full length, because the magnetic field lines switch back after crossing the shock.

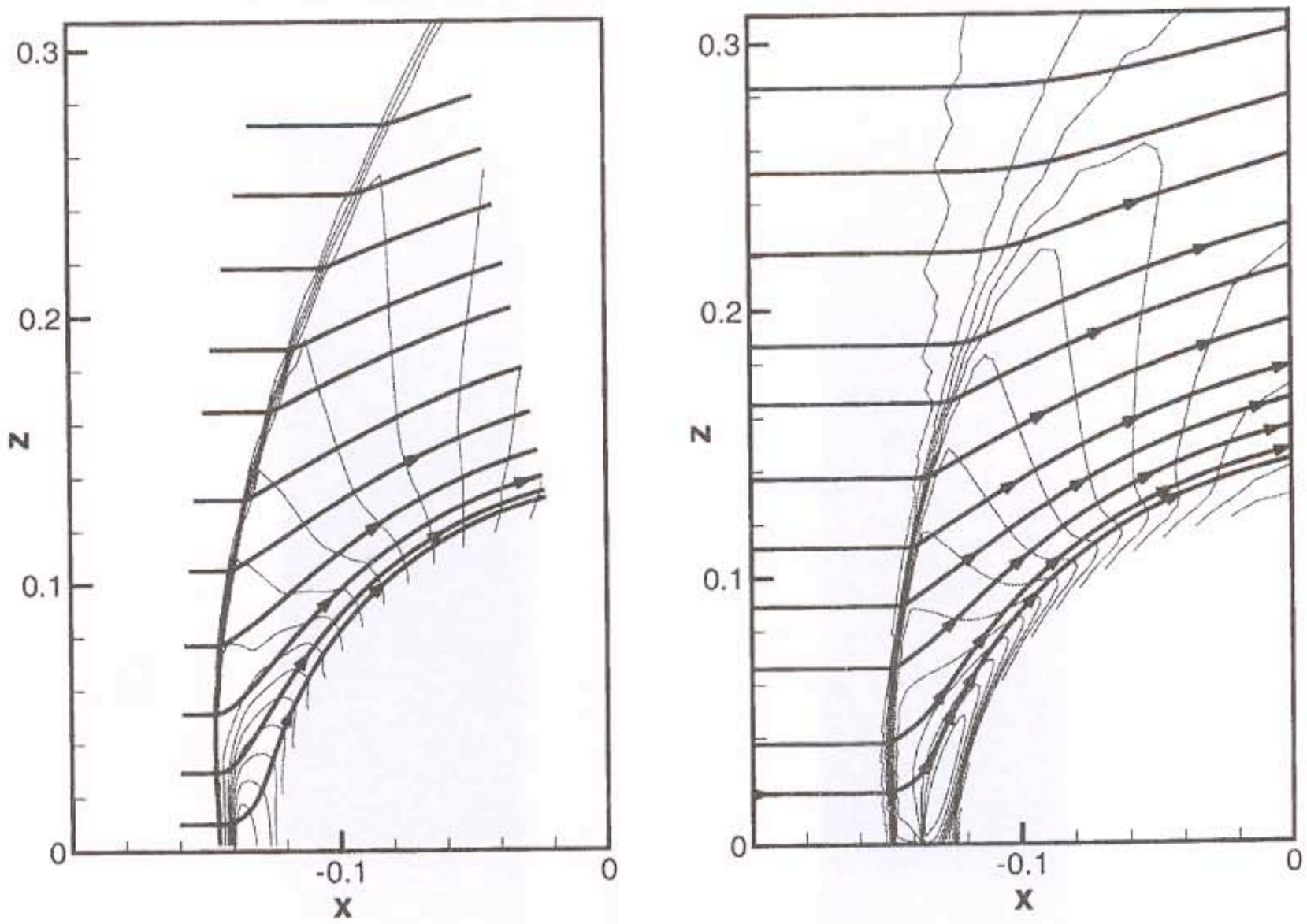

Fig. 12 Solution of the 3D bow shock flow in the plane $y = 0.02$ parallel to the $x - z$ symmetry plane computed by the $\mathcal{FV}$ (left) and the $\mathcal{RD}$ (right) schemes. Density contours are superimposed by the magnetic field lines.